ACS APPLIED MATERIALS & INTERFACES

Research Article

www.acsami.org

Selective Gas Diffusion in Graphene Oxides Membranes: A Molecular Dynamics Simulations Study

Shuping Jiao[†] and Zhiping Xu*[,†,‡]

[†]Applied Mechanics Laboratory, Department of Engineering Mechanics, and Center for Nano and Micro Mechanics, Tsinghua University, Beijing 100084, China

[‡]State Key Laboratory of Mechanics and Control of Mechanical Structures, Nanjing University of Aeronautics and Astronautics, Nanjing 210016, China

Supporting Information

ABSTRACT: Designing membrane materials from one-atom-thick structures is highly promising in separation and filtration applications for the reason that they offer the ultimate precision in modifying the atomic structures and chemistry for optimizing performance, and thus resolving the permeation-selectivity trade-off. In this work, we explore the molecular dynamics of gas diffusion in the gallery space between functionalized graphene layers as well as within nanopores across the multilayers. We have identified highly selective gas permeation that agrees with recent experimental measurements and is promising for advancing gas separation technologies such as hydrogen separation, helium/nitrogen generation, and CO_2 sequestration. The roles of structural and chemical factors are discussed by considering different types of gases including H_2, He, CH_4, N_2, O_2, CO, CO_2, and H_2O. The overall performance of graphene oxide membranes is also discussed with respect to their microstructures, and compared with recent experimental measurements. These understandings could advise high-performance gas-separation membrane development by engineering assemblies of two-dimensional layered structures.

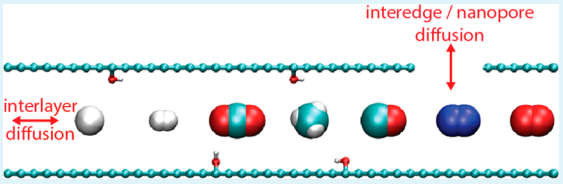

KEYWORDS: *graphene, graphene oxides, membrane, diffusion coefficients, gas separation, molecular dynamics simulations*

INTRODUCTION

Gas separation plays an important role in many industry processes including carbon dioxide (CO_2) sequestration, hydrogen (H_2) production, gas separation and purification.[1] Since the 1980s, membrane gas separation becomes popular as a commercial process on a grand scale because of its low energy cost, avoider of chemical progress, flexible structures and other merits. In traditional membrane materials used for gas separation, such as carbon, silica, silicon carbide, polymers, metal−organic framework (MOF),[2] the process to separate the gas mixture is based on their selective adsorption, orders of magnitude difference in the permeability of gases and vapors, or molecular-sieving mechanisms. From a design viewpoint to maximize the membrane performance, one should consider the trade-off between gas permeability and selectivity by optimizing the material microstructures and chemistry.[3] The increase of pressure-drop across the membrane and the energy consumption with its thickness suggests the superiority of using ultrathin membranes. However, to maintain their structural integrity during the operation, remarkable mechanical resistance to the pressure load must be assured. Graphene and related materials it derives are considered as excellent membrane materials in various applications by its nature of single-atom thickness,[4] as well as excellent mechanical resistance, and chemical stabilities.[5] Functionalized graphene, such as the graphene oxide (GO), provides additional opportunities in membrane material design at the atomic scale by tuning functional groups and defects in a rational way. As a result, ultrathin graphene and GO membranes have found promising applications in the field of membrane gas separation.

Recent experiments show that centimeter-sized, single-crystal graphene can be synthesized by chemical vapor deposition methods (CVD).[6] Though single-crystalline graphene is almost impervious for all molecules and ions, nanoscale pores created by exotic treatments could selectively transport guest molecules and ions.[7−9] On the other hand, nanoscale porous or channeled microstructures formed in graphene and GO membranes allow molecule and ion permeation at different rates.[10−15] In these multilayered, single-atom-thick sheets, microstructures such as defects including nanoholes, wrinkles, interedge slits, tears, as well as surface functional groups, the stacking order between neighboring sheets, and the interlayer spacing could be utilized to modulate the gas permeability and selectivity.[10,11] However, because of the complexity of the microstructures, the structure-performance correlation cannot be analyzed in detail by experimental measurements conducted at the membrane level, and a molecular-level study to clarify the role of above-mentioned controlling factors in the selective gas transport process is necessitated.

To this end, we perform molecular dynamics (MD) simulations to explore the dynamics of gas diffusion confined in the two-dimensional (2D) gallery between graphitic layers,

Received: December 22, 2014
Accepted: April 14, 2015
Published: April 14, 2015

DOI: 10.1021/am509048k
ACS Appl. Mater. Interfaces 2015, 7, 9052−9059

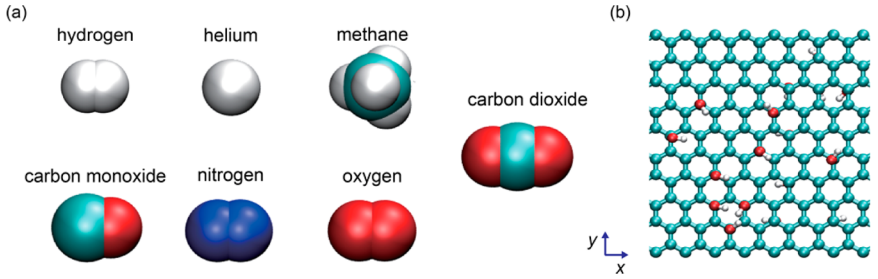

Figure 1. Atomic structures of (a) gas molecules including H_2, He, CH_4, CO, N_2, O_2, and CO_2. The gas molecules are plotted according to their atomic van der Waals radii. (b) Graphene oxide functionalized with hydroxyl groups.

which is the dominant mechanism of gas permeation because of the narrow pore size of ~1 nm.[16] We consider structural factors such as the interlayer spacing, intralayer pore size, and geometries of gas molecules, as well as the chemistry of both the gases and GO layers (e.g., atomic charges, dipoles etc.) in the study.

MODELS AND METHODS

Atomic Structures. The molecular structure of GO under investigation consists of hydroxyl, epoxy, and carbonyl groups on the basal plane, as well as defective sites and open edges functionalized by carboxyl, carbonyl, and phenol groups.[17] The hydroxyl groups are able to stay rich in the long-living quasi-equilibrium state according to the experimental evidence. They are thus discussed in our work, although comparison with the epoxy groups is made, which are also widely characterized in GO.[17−19] For oxidized regions in the atomistic GO model, we construct hydroxyl- and epoxy-functionalized graphene on both sides of the sheet with concentrations $c = n_O/n_C = 20\%$. Here n_O and n_C are the numbers of oxygen-rich groups and carbon atoms. Experimental studies report that a typical fraction of oxygen-rich functional species relative to the amount of carbon atoms in GO is ~20%.[17] Further reduction could yield lower concentrations (13.9−15.9%) in the reduced graphene oxide (RGO).[20] The spatial distributions of hydroxyl and epoxy groups are sampled randomly in the oxidized region. The model is illustrated in Figure 1. In this work, we define the interlayer distance as the distance between neighboring carbon basal planes, which is controlled in the simulations.

Interatomic Interaction Models and Molecular Dynamics Simulation. Classical molecular dynamics (MD) simulations are performed using the large-scale atomic/molecular massively parallel simulator (LAMMPS).[21] The all-atom optimized potentials for liquid simulations (OPLS-AA) are used for GO, which can capture essential many-body terms in interatomic interactions, including bond stretching, bond angle bending, nonbonding van der Waals and electrostatic interactions.[22] This force field was applied in a study of the pH-dependent behavior of GO aqueous solutions and was successfully validated by showing consistence with the experimental results.[22]

The interaction between gas molecules and graphene or GO sheets includes both van der Waals and electrostatic terms. The former one is described by the 12−6 Lennard−Jones potential $V_{LJ} = 4\varepsilon[(\sigma/r)^{12} - (\sigma/r)^6]$ as a function of the interatomic distance r, with parameters listed in Table 1, which were widely used in studying the diffusion and absorption of gases in porous medium such as silicalites.[23,24] The nonpolar CH_4 and He molecule are modeled as single spherical particles, and a rigid simple point charge effective pair (SPC/E) model is used for the water molecules.[24−26] H_2 molecules are modeled using a three-site model where the quantum contribution is included through quadrupolar interactions. This model has been successfully applied in studying hydrogen adsorption in carbon nanostructures and MOFs.[27,28] O_2, N_2, CO and CO_2 molecules in the gas phase are modeled using the transferable potentials for phase equilibria-explicit hydrogen (ThaPPE-EH) model with an additional point charge site.[29,30] The parameters used for their intermolecular interactions were validated by successfully describing the vapor−liquid coexistence and phase equilibria of their mixture.[29,30] The parameters for the van der Waals interactions between these gases and carbon, oxygen atoms in graphene, or GO are calculated from their own parameters using the Lorentz−Berthelot mixing rules.[31]

Table 1. Parameters for the 12−6 Lennard−Jones Potential and Partial Electric Charges Used in the Simulations for the Gas Molecules

molecule	site	ε/k_B (K)	σ (nm)	q (e)	bond length (nm)	ref
He	He	10.223	0.228	0.0		23
H_2	H	0.0	0.0	0.468	$l_{H=H}$ = 0.074	28
	COM*	36.7	0.2958	−0.936		
CH_4	CH_4	147.9	0.373	0.0		23
CO_2	C	27.0	0.280	+0.70	$l_{C=O}$ = 0.116	30
	O	79.0	0.305	−0.35		
N_2	N	36.0	0.331	−0.482	$l_{N=N}$ = 0.110	30
	COM*	0.0	0.0	+0.964		
O_2	O	49.048	0.3013	−0.123	$l_{O=O}$ = 0.121	29
	COM*	0.0	0.0	+0.246		
CO	C	52.888	0.343	+0.107	$l_{C=O}$ = 0.114	30
	O	30.219	0.312	−0.107		
epoxy	C	34.917	0.33997	+0.2	$l_{C=O}$ = 0.141	19
	O	71.561	0.29	−0.4		
hydroxyl	C	34.917	0.33997	+0.1966	$l_{C=O}$ = 0.141	19
	O	70.407	0.3166	−0.5260	$l_{O=H}$ = 0.0945	
	H	0	0	+0.3294		
carboxyl	C1**	34.917	0.33997	0.08	l_{C1-C} = 0.163	22
	C	53.671	0.375	0.55	$l_{C=O}$ = 0.124	
	O	107.343	0.296	−0.50	l_{C-O} = 0.142	
	O	86.896	0.300	−0.58	l_{O-H} = 0.100	
	H	0	0	0.45		

*COM: center of mass site. **C1: the carbon atom bonded to carboxylic group.

The nature of nanoconfined molecular dynamics depends critically on the molecule-solid interaction that should be validated as well. One of the key parameters to characterize the interfacial interaction is the water contact angle (WCA). The above-mentioned set of simulation parameters, ε_{C-O} = 4.063 meV, σ_{C-O} = 0.319 nm, predicts a WCA of $\theta_{c,G}$ = 98.4° for graphene that is in consistence with experimental measurements.[32] The WCA for GO, $\theta_{c,GO}$, is lower than $\theta_{c,G}$, and decrease with c − the concentration of oxygen-rich functional groups. For a typical value of c = 20% for GO, the simulation results is $\theta_{c,GO}$ = 26.8°, which is also close to recent experimental measurements.[33] This consistence validates that the choices of OPLS-AA and SPC/E force fields and parameters used in our MD simulations offer reliable predictions for graphene and GO sheets interacting with water

DOI: 10.1021/am509048k
ACS Appl. Mater. Interfaces 2015, 7, 9052−9059

molecules. Because the interactions between graphene, GO, and the gas molecules explored in this work share the same nature of van der Waals and electrostatic forces as that with water molecules, we expect this set of interatomic interaction models can yield reliable predictions for their structural and diffusive dynamics.

The atomic structures are equilibrated in a NVT ensemble using the Nosé-hoover thermostat at 300 K. All subsequent MD simulations are performed under the same thermodynamic control. Periodic boundary conditions (PBCs) are applied in all directions, consisting of supercells for graphene or GO sheets with length and width of 20 nm. This dimension of supercell is shorter than the mean free path of molecules under investigation in their gas phase at ambient conditions. We explore single-file diffusion here without consideration of their collective behaviors. The van der Waals forces are truncated at a distance of 1.2 nm with a constant shift in the energy over the whole range to remove the discontinuity. The long-range Coulomb interactions are computed by using the particle−particle particle-mesh algorithm (PPPM).[34] The time step for the equation-of-motion integration is 1 fs. The SHAKE algorithm is applied for the stretching terms between oxygen and hydrogen atoms in the oxygen-rich groups to reduce high-frequency vibrations that require a very short time step.

Diffusion Coefficient Calculations. For the self-diffusion of gas molecules in an isotropic medium, the diffusion coefficient can be evaluated from their trajectory by using the Einstein's definition relating the correlation function of atomic positions $\mathbf{r}$ to the diffusivity $D = \lim_{t\to\infty}(\langle|\mathbf{r}(t) - \mathbf{r}(0)|^2\rangle/2d_i t$, or the Green−Kubo relation using the velocity autocorrelation function $D = \int_0^\infty \langle \mathbf{v}(0)\mathbf{v}(t)\rangle dt/d_i$. Here d_i is the dimension of space, t is the simulation time and $\langle\rangle$ is the ensemble average. In our simulations of a few nanoseconds, the mean-square displacement (MSD) $\langle|\mathbf{r}(t) - \mathbf{r}(0)|^2\rangle$ is calculated on the basis of the time-series of all atomic positions, with the average taken from different starting points in the series.[31] For our system of gas molecules diffusing in the interlayer gallery of graphitic multilayers, the motion is anisotropic and more constrained in the normal direction of graphitic layers compared to the in-plane directions, so only the in-plane diffusivity is considered in this work with $d_i = 2$. Considering the trade-off between the computational consumption and quality of diffusion constant calculations, the time-averaging of MSD is performed every 10 or 40 ps through a ten-thousand-record time series in the thermal equilibration state for gas molecules diffusing within GO and graphene membranes, which is validated by yielding an almost linear relation between the MSD and t. The diffusivity D can then be reliably evaluated by fitting the data using the Einstein's relation.

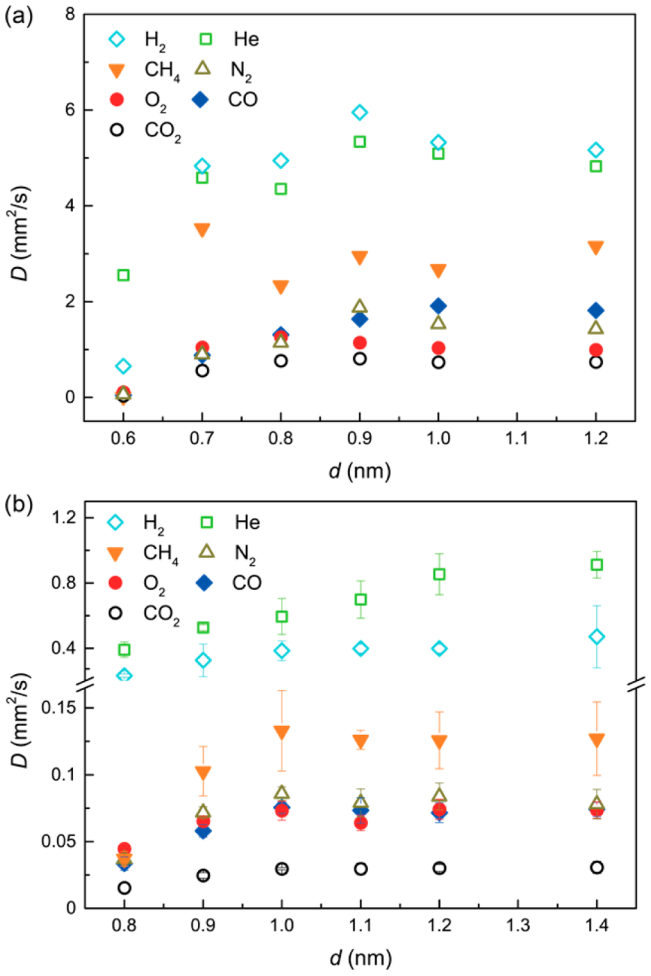

Figure 2. Dependence of gas diffusion coefficients D on the interlayer distance d for multilayered (a) graphene and (b) GO membranes. The error bars in panel (b) are plotted by the variance in the four GO samples with different distribution of oxidation groups at the same concentration $c = n_{OH}/n_C = 20\%$.

RESULTS AND DISCUSSION

Diffusion Coefficients of Gas Molecules between Graphene and GO Sheets. To quantify the gas diffusivity within the interlayer gallery between graphene or GO sheets, we calculate the diffusion coefficient D for different types of gas molecules. The interlayer distance d is tuned in the range of 0.6−1.2 nm and 0.8−1.4 nm, respectively. The results are summarized in Figure 2, from which we can see that in both cases D first increases with d and then approaches a constant as the interlayer spacing increases. The peak values read from the data in Figure 2 indicate the optimal distance for maximizing the gas diffusion rate. The convergence of D at large values of d indicates that the interlayer gallery no longer applies a constraint on the diffusion of gas molecules. Instead the gas molecules are adsorbed onto one of the sheet at a distance of ∼1 nm. Our MD simulations with different gas molecules diffusing on the surface of graphene or GO sheets confirm this explanation by yielding the same values of D as those calculated for gas molecules confined by sheets separated at a large interlayer distance. This fact can also be seen from the spatial distribution of gas molecules within the channel. To see this, we plot the density distribution profile of intercalated CO_2 within the 2D channel along the thickness direction for illustration (Figure 3). The profile features a single peak in the middle of the interlayer galley for $d = 0.8$ and $d = 0.9$ nm. As d increases, this peak splits into two symmetric ones and their distances to the GO sheet does not change much and remains as a constant for $d \geq 1.1$ nm, which suggests that the molecule adheres to one of the sheet at large interlayer distances instead of diffuses in the central region of channel that is free from the interaction from graphene or GO sheets. Results for other molecules demonstrate the same feature.

The MD simulation results show that, in general, gas molecules between graphene layers diffuse much faster than those in the GO multilayers, due to the atomistical smoothness and charge-neutrality of graphene that give rise to a flattened potential surface for gas diffusion. There are, however, some common trends observed in both cases. Between either GO or graphene layers, the He atom and hydrogen molecules with the smallest sizes diffuse the fastest, CH_4 takes the second place, the linear and polar CO_2 molecule diffuses the most slowly, and the diatomic molecules CO, N_2, O_2 have similar diffusion coefficients in between. The peak diffusion coefficients of different gas species at large interlayer distances differ by 2

DOI: 10.1021/am509048k
ACS Appl. Mater. Interfaces 2015, 7, 9052−9059

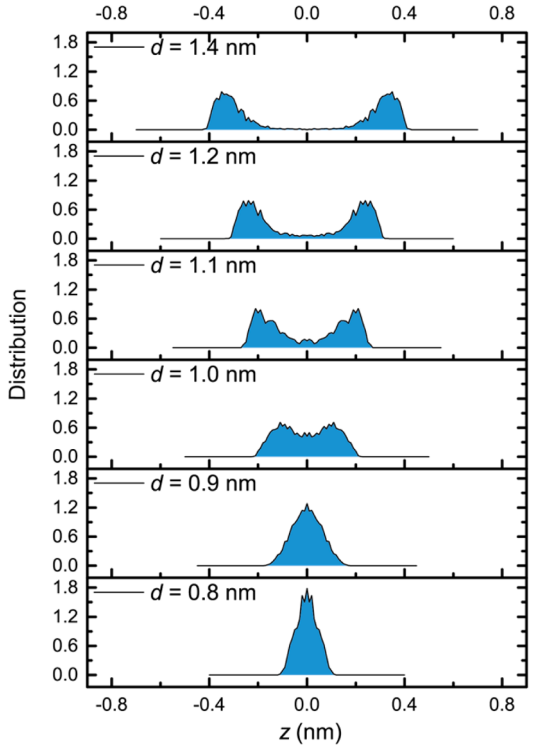

Figure 3. Density distribution profiles of the CO_2 molecule in the GO channels along the membrane thickness direction, with the interlayer distance d annotated. z is the position along this direction and $z = 0$ corresponds to the middle position.

orders in the GO membrane, but only 1 order for that between graphene layers.

These findings of high gas-selective diffusivity can be explained by a combined effect of three key factors: the size and shape of gas molecules, and their interactions with the GO or graphene sheets. We visualize the gas molecules by their sizes defined by the van der Waals radii (Figure 1). It is distinct that the molecules we explore here feature remarkable difference in their sizes and shapes, which are expected to play important roles in determining the diffusivity. The helium atom and hydrogen molecules diffuse faster than others because of its smallest size and weakest interaction with GO and graphene sheets. The CO_2 molecule shows the lowest diffusivity in general because of its large size and strong binding to the graphene/GO sheets. However, size is not the only controlling geometrical factor. The simulation results show that the diffusivity of CO_2 is significantly lower than that of CH_4 confined between graphene layers at an interlayer distance d larger than 0.6 nm. However, their difference diminishes as the interlayer diffusion channel becomes narrower. Specifically, our additional simulations show that, for $d = 0.55$ nm, the diffusivity of CH_4 becomes zero, while CO_2 molecule can still diffuse with a value of $D = 1.48 \times 10^{-3}$ mm^2/s (Figure S1 in the Supporting Information). This is because that the CO_2 molecule is linear and thus it could align along the interface to diffuse in very narrow channels. In contrast, the CH_4 molecule is spherical and its motion will be blocked at a relatively larger value of d, although it has a weaker binding with the graphene sheet compared to CO_2.

The charges and dipoles possessed by the atoms or molecules also affect the diffusion coefficients. For comparison,

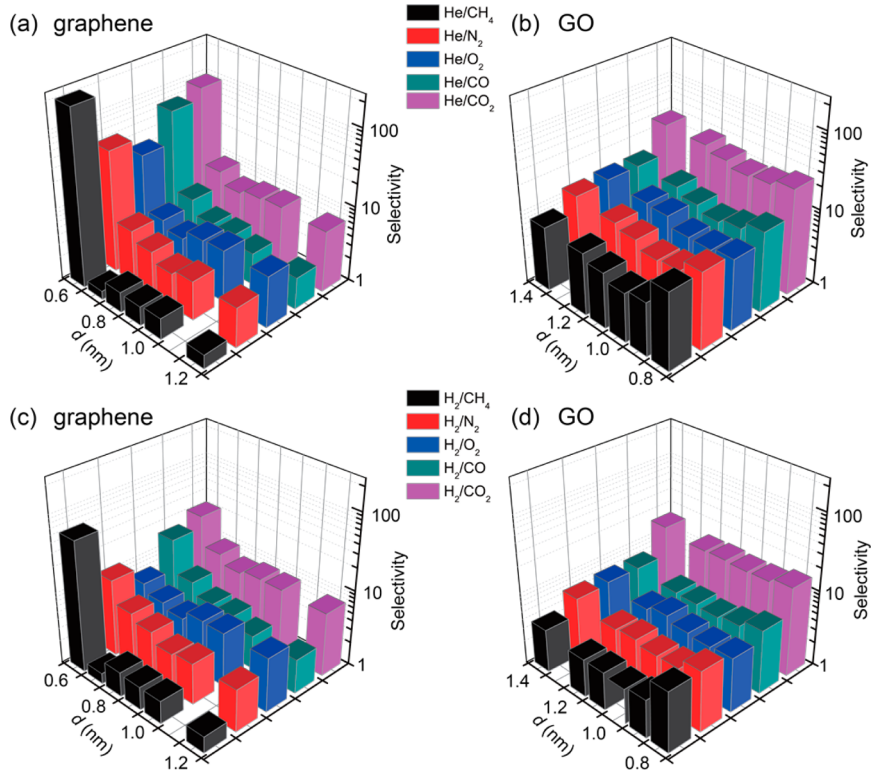

Figure 4. Selectivity of (a, b) He and (c, d) H_2 diffusion with respect to other gas molecules explored in this study for (a, c) graphene and (b, d) GO membranes. Here the selectivity is defined as $S = D_{He/H2}/D$, where $D_{He/H2}$ and D are the diffusion coefficients of He atom and other gas molecules, respectively.

DOI: 10.1021/am509048k
ACS Appl. Mater. Interfaces 2015, 7, 9052−9059

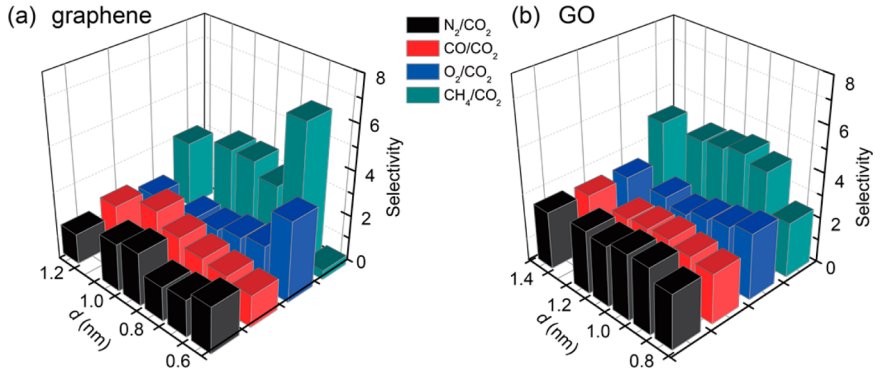

Figure 5. Selectivity of CO_2 diffusion with respect to other gas molecules explored in this study for (a) graphene and (b) GO membranes. Here the selectivity is defined as $S = D/D_{CO2}$, where D_{CO2} and D are the diffusion coefficients of the CO_2 molecule and other gas molecules, respectively.

the diffusion of CH_4 is always faster than CO_2 within GO the membrane, with an interlayer distance d ranging from 0.8 to 1.4 nm (Figure 2b). Our additional simulation results show that the diffusivities of CO_2 and CH_4 are still comparable at d = 0.6 nm (Figure S2 in the Supporting Information), in contrast to the results for graphene. We explain this observation by the presence of oxidation groups on GO, which gives rise to an energy barrier for the diffusion of all gas molecules, and the effect is strong for CO_2 because of its polarized nature. This electrostatic-interaction-induced difference in gas diffusivity would thus yield a remarkable selectivity for CO_2 diffusion in the GO membrane. We also study the diffusion of CH_4 and CO_2 on GO functionalized by epoxy groups rather than the hydroxyl. In epoxy, the van der Waals interaction between gas and the oxygen atoms is weaker, and the atomic charge of oxygen $q_O = -0.4e$ is lower that $-0.526e$ in the hydroxyl group. Our MD simulation results demonstrate that due to these facts, hydroxyl groups are more resistive to the gas diffusion, and the diffusion coefficients for both molecules increase significantly, by 150% and 203% at d = 1 nm. It should be remarked here that our previous discussion is to address the self-diffusion coefficients of single gas molecules and the collective effect is not included. We thus perform an additional set of simulations with 10 molecules in our system or a density of molecules n = 0.025 nm^{-2}. The simulation results show that CO_2 molecules aggregate and form clusters, which elevate the diffusion coefficient by ~50% at d = 1 nm. In contrast, CH_4 molecules are still dispersion in the gallery and the diffusivity remains less changed due to its unpolarized nature.

Selectivity of Gas Diffusion. We characterize the contrast between diffusivities of the molecules by analyzing the relative selectivity of He, H_2 and CO_2 diffusion compared to the others. We define the selectivity of molecule A with respect to another molecule B as $S_{A/B} = D_A/D_B$, where D_A and D_B are the diffusion coefficients calculated for species A and B. The results are summarized in Figure 4 and 5 for He, H_2 and CO_2, respectively. In the interlayer gallery of GO membranes, the selectivity of He/CO_2 can reach a value as high as 30, which is 4.5 for CH_4/CO_2 and in the range of 2−3 for CO/CO_2, N_2/CO_2, O_2/CO_2. On the other hand, the selectivities of He/CO, He/O_2, He/N_2 range from 8 to 12. The value of $S_{CH4/CO2}$ ranges from 4 to 10, which changes with the interlayer distance. In contrast, between the graphene layers, the values of selectivity for N_2/CO_2, CO/CO_2, O_2/CO_2 are slightly lower than that in GO, in the range between 1 and 3. The selectivity for He/N_2, He/CO, He/CH_4, He/O_2, He/CO_2 is also slightly lower than that in GO except for the situation with a small interlayer distance of d = 0.6 nm. The behavior of H_2 is generally similar as He, although H_2 diffuse more slowly than He between GO layers.

Gas Diffusion in the GO Membrane with Patterned Functional Groups. There are evidence from experimental reports that the functionalization groups on graphene prefer to cluster into patches with typical sizes of 1−2 nm, to lower their formation energy.[35−39] As a result, the interlayer gallery between GO sheets in the membrane could be considered as a composite consisting of pristine and oxidized graphene sheets. To explore gas diffusion in this more realistic situation, we perform additional MD simulations with this type of one-dimensional "superlattice" composed by aligned graphene and GO channels with widths of about 2 nm. The diffusion coefficients are then calculated along directions both in parallel to and perpendicular with the channel. Our simulation results show that although the atomic structure of this hybrid channel is anisotropic, the diffusion coefficients in these two directions are almost the same for the whole 2D channel with the patch size of 1−2 nm, although the mass diffusion is more efficient in the channel between pristine graphene regions than that between oxidized regions at the same interlayer distance. Thus, the value of D could be estimated by performing an area-based average based on the sizes of pristine and oxidized regions.

Role of the Humidity and Gas Solubility. The diffusion of water molecules between graphene and GO layers is also explored in this work. Our simulation results show that between graphene layers, the diffusion coefficient varies between 1.47 and 6.40 mm^2/s depending on the interlayer space which rank only second to He. However, when intercalated between GO sheets, D decreases to 1.21×10^{-4} to 8.42×10^{-4} mm^2/s, which is much lower than other gases explored and thus is not included in our previous discussion. Sharing the similar polar feature as CO_2, the tetrahedral topology of the OH bonds and long pairs in the H_2O molecule could lead to the formation of a hydrogen bond (H-bond) network with the oxygen-rich groups in GO. Moreover, due to the hydrophilic nature of GO, its interlayer gallery could easily be filled by water molecules, which change the interlayer distance from 0.7 to 1.2 nm.[40,41]

With the presence of intercalated water, the gas solubility becomes another determining factor for gas diffusion with graphene or GO membranes, especially for gases that are highly soluble, such as CO_2. For example, recent first-principles calculations show that water molecules inside the interlayer space of GO could trap CO_2 molecules.[42] To investigate the role of humidity in the gas transport, we simulate the gas diffusion with the presence of water between GO layers with

DOI: 10.1021/am509048k
ACS Appl. Mater. Interfaces 2015, 7, 9052−9059

patterned functional group. Water molecules occupy the full gallery including both the pristine and oxidized regions. The simulation results show a notable decline in the diffusivity (Table 2), and thus we conclude that high humidity will block the gas diffusion seriously. Though, some experiments report better permeance of CO_2 through high humidity membrane that may owe to the higher solubility of CO_2 than most other gas molecules.

Table 2. Diffusion Coefficients between GO Sheets with the Presence of Water[a]

	He	CH_4	CO_2
D_{H2O} (mm^2/s)	0.0312	0.0065	0.006575
D (mm^2/s)	1.5735	0.4233	0.05575
D/D_{H2O}	50.43	65.13	8.48

[a]Here D_{H2O} and D are the diffusion coefficients of gas molecules in the patterned channel with and without water intercalation, respectively. The interlayer spacing of both channels is 1 nm.

Design of Separation Membranes with Layered Structures. We now discuss the practical applications of using graphene and GO membranes for gas separation and purification based on our simulation results. It should be noted here that the gas selectivity in these applications comes mainly from the difference in gas permeability, which is determined by the diffusivity (kinetic factor) and solubility (or sorption, thermodynamic factor).[43] However, as the consideration of solubility of gases in graphene or GO membranes is out of scope in this work and we restrict our discussion with respect to the diffusivity only.[44] From the data in Figures 4 and 5 we conclude that the graphene membrane with an interlayer spacing of ~0.6 nm shows both high selectivity and permeability for He and H_2 separation. On the other hand, the GO membrane features more excellent performance for removing CO_2 from other gas species in most interlayer distance, although the diffusion coefficients of all gas molecules are about 1 order of magnitude lower than the values in the graphene membrane with the same interlayer distance. The interlayer distance between graphene or GO layers could be tuned by intercalations. Although water filling was reported to be able to expand the interlayer gallery of these membranes, it will reduce the gas diffusivity significantly as we discussed earlier. Other types of low-density intercalations such as polymers or interlayer cross-links may be used to engineer the interlayer distance.[45,46] Moreover, the presence of wrinkles and nanochannels that form naturally during the membrane fabrication or engineered by nanostrand-templating offers another strategy to tune the microstructures of graphene or GO membranes to establish optimized separation performance.[47]

Compared to Recent Experimental Results. Recently, a few experimental measurements have been conducted to quantify the gas diffusion and selective transport across membranes of GO monolayer with defects or multilayers with thickness of several nanometers.[12−15] Overall speaking, the interlayer diffusion could be the rate-limiting process compared to the cross diffusion through nanopores or interedge spaces within the graphene or GO layers, considering the high aspect ratio of these 2D sheets. The lateral size of the 2D diffusion channel is on the order of micrometers, while the interlayer distance is three orders shorter. Thus, the excellent gas selectivity reported could be correlated with the contrast in interlayer diffusivities we explore here.[12,13] Actually, the high selectivity of $He/CO_2 \approx 30$ reported by these experimental work is close to our simulation results. More specifically, the gas penetrance and selectivity is demonstrated to depend on the stacking order of GO sheets when assembled into the GO membrane, indicating that the 2D diffusion between the GO interlayer contributes to the gas transport.[12] In another report, the measured permeability shows the order as predictions for the self-diffusivity from our MD simulations, i.e., He, H_2 > CH_4 > O_2, N_2, CO > CO_2. It should be noted that this order is not coincident with the kinetic diameters of the gas molecules d_k as commonly thought for the gas transport in porous materials. This finding indicates that the kinetic diameters of gas molecules may not be the sole determining factor for the permeability. Gas molecules featuring smaller kinetic diameters could travel even faster than those with larger d_k, especially when the driving pressure is relatively low, where the chemistry of solid walls and their interaction with the gas molecules becomes more dominant in the gas diffusion than the kinetic factors. This conclusion is also agreed by previous studies on other molecule-sieving membranes such as the MOFs.[48]

From our MD simulation results we also conclude that as the channel width increases beyond ~1 nm, gas molecules preferred to adhere to the graphene or GO walls. However, as the width further increase and the surface of the walls are highly occupied. Then more molecules start to occupy the interlayer gallery. As a result, the kinetic factors could become more important as additional gas diffusion in the central part of the channel could be more efficient than that on the surface where gas-surface interaction dominants. However, we should also point out that the underlying mechanisms of the selective gas transport cannot be fully understood unless the complex microstructures of GO membranes and the multiple factors influencing the diffusion are resolved as we have discussed in this work. More information about the microstructures of membranes and further examination of their gas separation performance are required to obtain more insights in elucidating the dominating factors. From a practical design point of view, a well-controlled microstructure of the membrane could also maximize the membrane performance.

Other Types of Channels in the Membranes of Multilayered Graphene or GO Sheets. Considering graphene and other 2D materials with monatomic thickness, there could be other channels in the membrane opened for gas transport. We now compare the interlayer diffusion to other diffusion paths, such as nanoholes created within the graphene or GO sheets by irradiation. The single-layer graphene membrane with nanoholes of 0.25 nm demonstrates a high H_2/CH_4 selectivity up to 1×10^8.[49−51] However, monolayer sheets are usually not very stable upon external perturbations such as the pressure applied in the separation process, especially as the hole density is increased for high permeability. Moreover, creating nanoholes with precisely controlled size and spatial distribution are difficult and costly. Thus, using multilayer sheets are more favored for practical considerations. For a related low density of nanoholes in the sheet, the performance of gas separation will be determined in a combined way for the network composed of both interlayer nanoholes and interlayer 2D channels.

To see this, we carry out MD simulations for gas diffusion through parallel slits between stacked GO sheets where the slit edges are functionalized by carboxylic groups with a line density of 0.815 nm^{-1}. The results summarized in Table 3 show that at

DOI: 10.1021/am509048k
ACS Appl. Mater. Interfaces 2015, 7, 9052−9059

Table 3. Diffusion Coefficients through Parallel Slits in GO Membranes, Where the Slit Edges Are Functionalized by Carboxylic Groups with a Line Density of 0.815 nm^{-1}

d (nm)	D_{He} (mm^2/s)	D_{H2} (mm^2/s)	D_{CH4} (mm^2/s)	D_{CO2} (mm^2/s)
0.9	0.1005	0.15015	0.010	0.00186
1.0	0.0915	0.1845	0.0125	0.00388
1.1	0.115	0.2325	0.0138	0.0065
1.2	0.12965	0.23915	0.0128	0.0105
1.4	0.2417	0.3809	0.011	0.01225

the same channel width, the coefficient of gas diffusion is much lower than that the interlayer diffusion between graphene or GO sheets. Considering in practice the interdge spaces can hardly be aligned across the whole membrane, the effective diffusivity could be further reduced by a significant amount. Nanopores within the sheets are also explored and shows even lower gas diffusivity due to the 2D steric confinement. For multilayer graphene or GO membranes, the interlayer diffusion could become the rate-limiting and species-selecting process even nanoholes are created as major diffusive channels across the membrane because the alignment between nanoholes in neighboring sheets can hardly be assured. As indicated from our MD simulation-based study, the controlling of interlayer distance and surface chemistry of the graphene and GO sheets offers a feasible approach in improving the performance.

CONCLUSION

In this work, we present our computational study on the gas diffusion in the interlayer gallery of graphene and GO membranes, which elucidates the molecular mechanisms of selective gas diffusion through nanoscale channles in graphene or GO membranes. The results show that by adjusting the interlayer spacing or chemical modification of the membrane, highly selective gas permeation could be established. The simulation results are in good agreement with recent experimental measurements, although more quantitative assessment of the predictions requires further information on the microstructural characteristics of the GO membranes. The underlying mechanisms of the selective gas transport are discussed with respect to the size, shape of molecules, the surface chemistry of graphene sheet and its interaction between the gas molecules. We also discussed practical issues in developing high-performance gas separation membranes by using monolayer 2D materials such as graphene and its derivatives as the building blocks, which hold the promise as the ultimate materials because of their excellent mechanical stability and capability of being engineered at the molecular level. We conclude that the rational design of the nanohole engineering for single sheets and staking order in the membrane assembly is necessitated to push the limit of performance trade-off between permeability and selectivity for monolayer material-based gas separation.

ASSOCIATED CONTENT

Supporting Information

Values of atomic van der Waals radii and van der Waals sizes of the gas molecules explored in this work, coefficients of gases diffusion between GO sheets functionalized by hydroxyl and epoxy groups, and time-dependent mean square displacements calculated from the MD simulations. The Supporting Information is available free of charge on the ACS Publications website at DOI: 10.1021/am509048k.

AUTHOR INFORMATION

Corresponding Author

*E-mail: xuzp@tsinghua.edu.cn.

Notes

The authors declare no competing financial interest.

ACKNOWLEDGMENTS

This work was supported by the State Key Laboratory of Mechanics and Control of Mechanical Structures (Nanjing University of Aeronautics and Astronautics) through Grant MCMS-0414G01, and the National Natural Science Foundation of China through Grant 11222217 and 11472150. The computation was performed on the Explorer 100 cluster system at Tsinghua National Laboratory for Information Science and Technology.

REFERENCES

(1) Paul, D. R.; Yampol'skii, Y. P. *Polymeric Gas Separation Membranes*. CRC Press 1993.

(2) Li, J.-R.; Ma, Y.; McCarthy, M. C.; Sculley, J.; Yu, J.; Jeong, H.-K.; Balbuena, P. B.; Zhou, H.-C. Carbon Dioxide Capture-Related Gas Adsorption and Separation in Metal-Organic Frameworks. *Coord. Chem. Rev.* **2011**, *255*, 1791−1823.

(3) Robeson, L. M. The Upper Bound Revisited. *J. Membr. Sci.* **2008**, *320*, 390−400.

(4) Meyer, J. C.; Geim, A. K.; Katsnelson, M. I.; Novoselov, K. S.; Booth, T. J.; Roth, S. The Structure of Suspended Graphene Sheets. *Nature* **2007**, *446*, 60−63.

(5) Lee, C.; Wei, X.; Kysar, J. W.; Hone, J. Measurement of the Elastic Properties and Intrinsic Strength of Monolayer Graphene. *Science* **2008**, *321*, 385−388.

(6) Hao, Y.; Bharathi, M. S.; Wang, L.; Liu, Y.; Chen, H.; Nie, S.; Wang, X.; Chou, H.; Tan, C.; Fallahazad, B.; Ramanarayan, H.; Magnuson, C. W.; Tutuc, E.; Yakobson, B. I.; McCarty, K. F.; Zhang, Y.-W.; Kim, P.; Hone, J.; Colombo, L.; Ruoff, R. S. The Role of Surface Oxygen in the Growth of Large Single-Crystal Graphene on Copper. *Science* **2013**, *342*, 720−723.

(7) Ozeki, S.; Ito, T.; Uozumi, K.; Nishio, I. Scanning Tunneling Microscopy of UV-Induced Gasification Reaction on Highly Oriented Pyrolytic Graphite. *Jpn. J. Appl. Phys.* **1996**, *35*, 3772.

(8) Huh, S.; Park, J.; Kim, Y. S.; Kim, K. S.; Hong, B. H.; Nam, J.-M. UV/Ozone-Oxidized Large-Scale Graphene Platform with Large Chemical Enhancement in Surface-Enhanced Raman Scattering. *ACS Nano* **2011**, *5*, 9799−9806.

(9) Hu, S.; Lozada-Hidalgo, M.; Wang, F. C.; Mishchenko, A.; Schedin, F.; Nair, R. R.; Hill, E. W.; Boukhvalov, D. W.; Katsnelson, M. I.; Dryfe, R. A. W.; Grigorieva, I. V.; Wu, H. A.; Geim, A. K. Proton Transport through One-Atom-Thick Crystals. *Nature* **2014**, *516*, 227−230.

(10) Huang, P. Y.; Ruiz-Vargas, C. S.; van der Zande, A. M.; Whitney, W. S.; Levendorf, M. P.; Kevek, J. W.; Garg, S.; Alden, J. S.; Hustedt, C. J.; Zhu, Y.; Park, J.; McEuen, P. L.; Muller, D. A. Grains and Grain Boundaries in Single-Layer Graphene Atomic Patchwork Quilts. *Nature* **2011**, *469*, 389−392.

(11) Duong, D. L.; Han, G. H.; Lee, S. M.; Gunes, F.; Kim, E. S.; Kim, S. T.; Kim, H.; Ta, Q. H.; So, K. P.; Yoon, S. J.; Chae, S. J.; Jo, Y. W.; Park, M. H.; Chae, S. H.; Lim, S. C.; Choi, J. Y.; Lee, Y. H. Probing Graphene Grain Boundaries with Optical Microscopy. *Nature* **2012**, *490*, 235−239.

(12) Kim, H. W.; Yoon, H. W.; Yoon, S.-M.; Yoo, B. M.; Ahn, B. K.; Cho, Y. H.; Shin, H. J.; Yang, H.; Paik, U.; Kwon, S.; Choi, J.-Y.; Park, H. B. Selective Gas Transport through Few-Layered Graphene and Graphene Oxide Membranes. *Science* **2013**, *342*, 91−95.

(13) Li, H.; Song, Z.; Zhang, X.; Huang, Y.; Li, S.; Mao, Y.; Ploehn, H. J.; Bao, Y.; Yu, M. Ultrathin, Molecular-Sieving Graphene Oxide Membranes for Selective Hydrogen Separation. *Science* **2013**, *342*, 95−98.

DOI: 10.1021/am509048k
ACS Appl. Mater. Interfaces 2015, 7, 9052−9059

(14) Celebi, K.; Buchheim, J.; Wyss, R. M.; Droudian, A.; Gasser, P.; Shorubalko, I.; Kye, J.-I.; Lee, C.; Park, H. G. Ultimate Permeation across Atomically Thin Porous Graphene. *Science* **2014**, *344*, 289−292.
(15) Boutilier, M. S. H.; Sun, C.; O'Hern, S. C.; Au, H.; Hadjiconstantinou, N. G.; Karnik, R. Implications of Permeation through Intrinsic Defects in Graphene on the Design of Defect-Tolerant Membranes for Gas Separation. *ACS Nano* **2014**, *8*, 841−849.
(16) Verweij, H.; Schillo, M. C.; Li, J. Fast Mass Transport through Carbon Nanotube Membranes. *Small* **2007**, *3*, 1996−2004.
(17) Kim, S.; Zhou, S.; Hu, Y.; Acik, M.; Chabal, Y. J.; Berger, C.; de Heer, W.; Bongiorno, A.; Riedo, E. Room-Temperature Metastability of Multilayer Graphene Oxide Films. *Nat. Mater.* **2012**, *11*, 544−549.
(18) Wei, N.; Peng, X.; Xu, Z. Breakdown of Fast Water Transport in Graphene Oxides. *Phys. Rev. E* **2014**, *89*, 012113.
(19) Wei, N.; Peng, X.; Xu, Z. Understanding Water Permeation in Graphene Oxide Membranes. *ACS Appl. Mater. Interfaces* **2014**, *6*, 5877−5883.
(20) Dreyer, D. R.; Park, S.; Bielawski, C. W.; Ruoff, R. S. The Chemistry of Graphene Oxide. *Chem. Soc. Rev.* **2010**, *39*, 228−240.
(21) Plimpton, S. Fast Parallel Algorithms for Short-Range Molecular Dynamics. *J. Comput. Phys.* **1995**, *117*, 1−19.
(22) Shih, C.-J.; Lin, S.; Sharma, R.; Strano, M. S.; Blankschtein, D. Understanding the pH-Dependent Behavior of Graphene Oxide Aqueous Solutions: A Comparative Experimental and Molecular Dynamics Simulation Study. *Langmuir* **2011**, *28*, 235−241.
(23) Skoulidas, A. I.; Sholl, D. S. Transport Diffusivities of CH_4, CF_4, He, Ne, Ar, Xe, and SF_6 in Silicalite from Atomistic Simulations. *J. Phys. Chem. B* **2002**, *106*, 5058−5067.
(24) Martín-Calvo, A.; Lahoz-Martín, F. D.; Calero, S. Understanding Carbon Monoxide Capture Using Metal−Organic Frameworks. *J. Phys. Chem. C* **2012**, *116*, 6655−6663.
(25) Xiong, W.; Liu, J. Z.; Ma, M.; Xu, Z.; Sheridan, J.; Zheng, Q. Strain Engineering Water Transport in Graphene Nanochannels. *Phys. Rev. E* **2011**, *84*, 056329.
(26) Falk, K.; Sedlmeier, F.; Joly, L.; Netz, R. R.; Bocquet, L. Molecular Origin of Fast Water Transport in Carbon Nanotube Membranes: Superlubricity Versus Curvature Dependent Friction. *Nano Lett.* **2010**, *10*, 4067−4073.
(27) Darkrim, F.; Aoufi, A.; Levesque, D. Quantum Contribution to Gas Adsorption in Carbon Nanotubes. *Mol. Simul.* **2006**, *24*, 51−61.
(28) Yang, Q.; Zhong, C. Molecular Simulation of Carbon Dioxide/Methane/Hydrogen Mixture Adsorption in Metal−Organic Frameworks. *J. Phys. Chem. B* **2006**, *110*, 17776−17783.
(29) Hansen, N.; Agbor, F. A. B.; Keil, F. J. New Force Fields for Nitrous Oxide and Oxygen and Their Application to Phase Equilibria Simulations. *Fluid Phase Equilib.* **2007**, *259*, 180−188.
(30) Potoff, J. J.; Siepmann, J. I. Vapor−Liquid Equilibria of Mixtures Containing Alkanes, Carbon Dioxide, and Nitrogen. *AlChE J.* **2001**, *47*, 1676−1682.
(31) Allen, M. P.; Tildesley, D. J. *Computer Simulation of Liquids*; Oxford University Press: New York, 1989.
(32) Wei, N.; Lv, C.; Xu, Z. Wetting of Graphene Oxide: A Molecular Dynamics Study. *Langmuir* **2014**, *30*, 3572−3578.
(33) Sun, P.; Zhu, M.; Wang, K.; Zhong, M.; Wei, J.; Wu, D.; Xu, Z.; Zhu, H. Selective Ion Penetration of Graphene Oxide Membranes. *ACS Nano* **2013**, *7*, 428−437.
(34) Hockney, R. W.; Eastwood, J. W. *Computer Simulation Using Particles*; Taylor & Francis: Oxford, U.K., 1989.
(35) Erickson, K.; Erni, R.; Lee, Z.; Alem, N.; Gannett, W.; Zettl, A. Determination of the Local Chemical Structure of Graphene Oxide and Reduced Graphene Oxide. *Adv. Mater.* **2010**, *22*, 4467−4472.
(36) Pacilé, D.; Meyer, J. C.; Fraile Rodríguez, A.; Papagno, M.; Gómez-Navarro, C.; Sundaram, R. S.; Burghard, M.; Kern, K.; Carbone, C.; Kaiser, U. Electronic Properties and Atomic Structure of Graphene Oxide Membranes. *Carbon* **2011**, *49*, 966−972.
(37) Zhou, S.; Bongiorno, A. Origin of the Chemical and Kinetic Stability of Graphene Oxide. *Sci. Rep.* **2013**, *3*, 2484.
(38) Kumar, P. V.; Bardhan, N. M.; Tongay, S.; Wu, J.; Belcher, A. M.; Grossman, J. C. Scalable Enhancement of Graphene Oxide Properties by Thermally Driven Phase Transformation. *Nat. Chem.* **2013**, *6*, 151−158.
(39) Wilson, N. R.; Pandey, P. A.; Beanland, R.; Young, R. J.; Kinloch, I. A.; Gong, L.; Liu, Z.; Suenaga, K.; Rourke, J. P.; York, S. J.; Sloan, J. Graphene Oxide: Structural Analysis and Application as a Highly Transparent Support for Electron Microscopy. *ACS Nano* **2009**, *3*, 2547−2556.
(40) Talyzin, A. V.; Hausmaninger, T.; You, S.; Szabo, T. The Structure of Graphene Oxide Membranes in Liquid Water, Ethanol and Water-Ethanol Mixtures. *Nanoscale* **2014**, *6*, 272−281.
(41) Talyzin, A. V.; Luzan, S. M.; Szabó, T.; Chernyshev, D.; Dmitriev, V. Temperature Dependent Structural Breathing of Hydrated Graphite Oxide in H_2O. *Carbon* **2011**, *49*, 1894−1899.
(42) Yumura, T.; Yamasaki, A. Roles of Water Molecules in Trapping Carbon Dioxide Molecules inside the Interlayer Space of Graphene Oxides. *Phys. Chem. Chem. Phys.* **2014**, *16*, 9656−9666.
(43) Rogers, W. A.; Buritz, R. S.; Alpert, D. Diffusion Coefficient, Solubility, and Permeability for Helium in Glass. *J. Appl. Phys.* **1954**, *25*, 868−875.
(44) Swope, W. C.; Andersen, H. C. A Molecular Dynamics Method for Calculating the Solubility of Gases in Liquids and the Hydrophobic Hydration of Inert-Gas Atoms in Aqueous Solution. *J. Phys. Chem.* **1984**, *88*, 6548−6556.
(45) Liu, Y.; Xie, B.; Xu, Z. Mechanics of Coordinative Crosslinks in Graphene Nanocomposites: A First-Principles Study. *J. Mater. Chem.* **2011**, *21*, 6707−6712.
(46) Liu, Y.; Xie, B.; Zhang, Z.; Zheng, Q.; Xu, Z. Mechanical Properties of Graphene Papers. *J. Mech. Phys. Solids* **2012**, *60*, 591−605.
(47) Huang, H.; Song, Z.; Wei, N.; Shi, L.; Mao, Y.; Ying, Y.; Sun, L.; Xu, Z.; Peng, X. Ultrafast Viscous Water Flow through Nanostrand-Channelled Graphene Oxide Membranes. *Nat. Commun.* **2013**, *4*, 3979.
(48) Keskin, S.; Sholl, D. S. Screening Metal−Organic Framework Materials for Membrane-Based Methane/Carbon Dioxide Separations. *J. Phys. Chem. C* **2007**, *111*, 14055−14059.
(49) Jiang, D.-e.; Cooper, V. R.; Dai, S. Porous Graphene as the Ultimate Membrane for Gas Separation. *Nano Lett.* **2009**, *9*, 4019−4024.
(50) Du, H.; Li, J.; Zhang, J.; Su, G.; Li, X.; Zhao, Y. Separation of Hydrogen and Nitrogen Gases with Porous Graphene Membrane. *J. Phys. Chem. C* **2011**, *115*, 23261−23266.
(51) Koenig, S. P.; Wang, L.; Pellegrino, J.; Bunch, J. S. Selective Molecular Sieving through Porous Graphene. *Nat. Nanotechnol.* **2012**, *7*, 728−732.

DOI: 10.1021/am509048k
ACS Appl. Mater. Interfaces 2015, 7, 9052−9059